Biomimetic collagenous scaffold to tune inflammation by targeting macrophages

Francesca Taraballi[1], Bruna Corradetti[1,2], Silvia Minardi[1], Sebastian Powel[1], Fernando Cabrera[1], Jeff L. Van Eps[1,3], Bradley K Weiner[1,4] and Ennio Tasciotti[1]

Abstract

The inflammatory response following implantation of a biomaterial is one of the major regulatory aspects of the overall regenerative process. The progress of inflammation determines whether functional tissue is restored or if nonfunctional fibrotic tissue is formed. This delicate balance is directed by the activity of different cells. Among these, macrophages and their different phenotypes, the inflammatory M1 to anti-inflammatory M2, are considered key players in the process. Recent approaches exploit macrophage's regenerative potential in tissue engineering. Here, we propose a collagen scaffold functionalized with chondroitin sulfate (CSCL), a glycosaminoglycan known to be able to tune inflammation. We studied CSCL effects on bone-marrow-derived macrophages in physiological, and lipopolysaccharides-inflamed, conditions in vitro. Our data demonstrate that CSCL is able to modulate macrophage phenotype by inhibiting the LPS/CD44/NF-kB cascade. As a consequence, an upregulation of anti-inflammatory markers (*TGF-β*, *Arg*, *MRC1*, and *IL-10*) was found concomitantly with a decrease in the expression of pro-inflammatory markers (*iNOS*, *TNF-α*, *IL-1β*, *IL-12β*). We then implanted CSCL subcutaneously in a rat model to test whether the same molecular mechanism could be maintained in an in vivo environment. In vivo data confirmed the in vitro studies. A significant reduction in the number of infiltrating cells around and within the implants was observed at 72h, with a significant downregulation of pro-inflammatory genes expression. The present work provides indications regarding the immunomodulatory potential of molecules used for the development of biomimetic materials and suggests their use to direct macrophage immune modulation for tissue repair.

Introduction

The stem cell niche of the injured tissue has been considered the ultimate target in tissue engineering for years.[1] A broad variety of biomaterials have been successfully developed to support proliferation, infiltration, or differentiation of allogeneic transplanted[2,3] or endogenous[4] stem cells to achieve functional tissue restoration. However, the stem cell niche is a very complex environment characterized by a multitude of key components, including the integral interactions between supporting and circulating cells, secreted growth factors, extracellular matrix composition, environmental signals (e.g. hypoxia), physical parameters (e.g. shear stress), and tissue stiffness.[5] Several tissue-engineering-based approaches have been developed to mimic the composition,[6,7] growth

factor presence and concentration,[8] and mechanical or physical environment[9] of the niche. A relatively lower but

[1]Department of Nanomedicine, Houston Methodist Research Institute, Houston, TX, USA
[2]Department of Life and Environmental Sciences, Università Politecnica delle Marche, Ancona, Italy
[3]Department of Surgery, Houston Methodist Hospital, Houston, TX, USA
[4]Department of Orthopedics & Sports Medicine, Houston Methodist Hospital, Houston, TX, USA.

Corresponding author:
Ennio Tasciotti, Department of Nanomedicine, Houston Methodist Research Institute, 6670 Bertner Ave., Houston, TX 77030, USA.
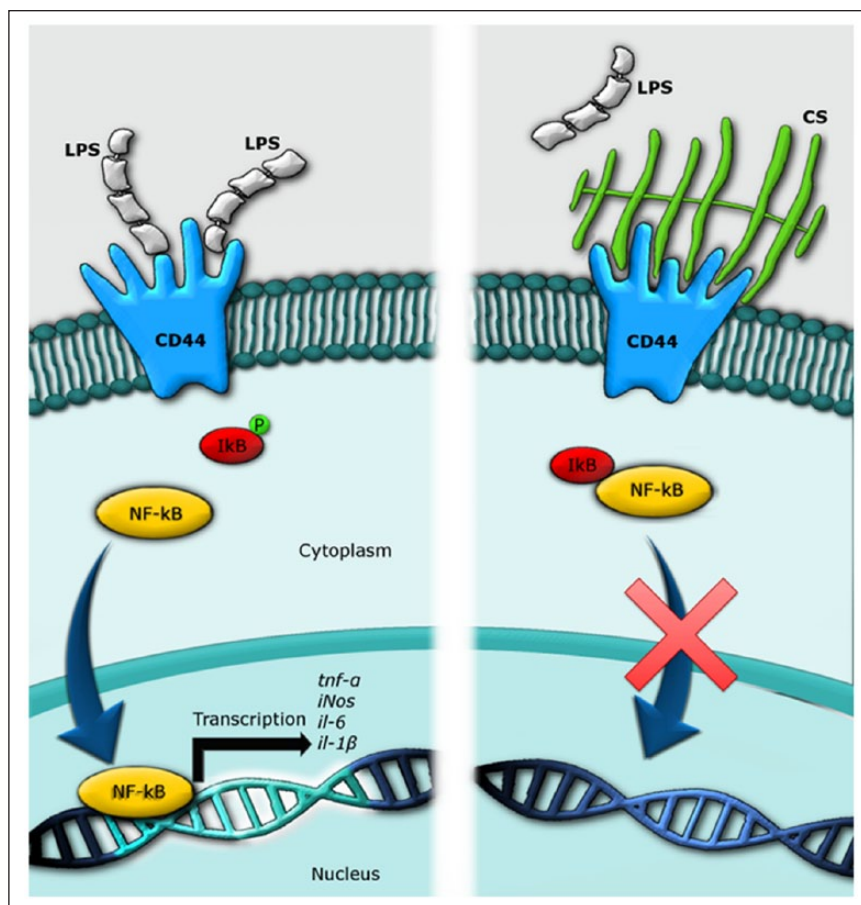Email: ETasciotti@houstonmethodist.org

Figure 1. Schematic representation of the mechanism activated by the CS (right side) to reduce the inflammatory response stimulated by LPS (left side). LPS binds its receptor on the macrophage's surface determining the phosphorylation of NF-kB factor. NF-kB translocates into the nucleus activating the transcription of pro-inflammatory genes (i.e. *IL-6*, *TNF-α*, *iNOS*, *IL-1β*). The presence of CS blocks the active site on the hyaluronic acid receptor impeding the LPS-CD44 bond, with the consequent inhibition of the LPS/CD44/NF-kB cascade.

growing number of works have exploited the role of the inflammatory response in tissue restoration[10] as a deep understanding of the inflammatory phases and a careful analysis of the key cellular players are required. Following biomaterial implantation, macrophages play a key role in the outcome of the healing and tissue regeneration processes.[11] This peculiar and very plastic cell type could enable a favorable healing response by encouraging functional tissue formation (M2 phenotype) or represent active antagonists to the regeneration process (M1 phenotype). This dual role is not absolute and, therefore, can be exploited, or actively targeted, to achieve complete functional tissue restoration.[12]

Recently, scientists are focusing their efforts in the development of smart strategies able to promote macrophage polarization to a pro-tissue healing phenotype with the aim of mitigating the adverse effects of biomaterial-induced inflammation.[13,14]

With this in mind, we recently developed a collagen scaffold functionalized with chondroitin sulfate (CS). CS

is a natural glycosaminoglycan that can be found in the extracellular matrix surrounding cells, especially in cartilage, skin, blood vessels, ligaments, and tendons, where it forms an essential component of proteoglycans.[15] Besides its structural function within the extracellular matrix, CS is well known for its immunomodulatory potential.[16] Specifically, it has been used as an anti-inflammatory molecule for the treatment of chronic diseases.[17] For example, CS has been reported to interfere with the activation of the hyaluronan receptor CD44 on chondrocytes and the macrophages in synovial fluid following articulation trauma.[18,19] CD44 is a transmembrane adhesion molecule responsible for enhancing the expression of pro-inflammatory markers by triggering the nuclear translocation of NF-kB.[20] In particular, CS pleiotropic effect seems to be due to its potential to inhibit the NF-kB nuclear translocation by competing with lipopolysaccharides (LPS) for the CD44 binding site, blocking the molecular cascade known to lead to the activation of the inflammatory status.[18] Figure 1 shows a schematic representation of the mechanism of

action CS plays in diminishing the nuclear translocation of NF-kB, normally triggered by LPS.

We hypothesized that the CS could exert the same anti-inflammatory potential even when immobilized onto a collagen-based scaffold. To test this hypothesis, we first evaluated its effect on primary bone-marrow-derived macrophages (BMDM) in an in vitro system. Specifically, we focused on two main phenomena occurring after the implant: the reaction to the material, which could lead to foreign-body reaction, and the capability of the material to contrast the inflammation induced by the surgery.

In the first case, we exposed BMDM to the material for 24 h and monitored changes in morphology and gene expression to understand whether or not CS was sufficient to modulate macrophages phenotype. In the second case, after defining the optimal conditions to inflame macrophages in vitro by testing different concentrations of LPS (10, 50, and 100 ng/mL) at different time points (48 and 72 h), we assessed the inflammatory response triggered when cells were cultured in the presence (CSCL) or absence collagen (CL) of CS. To understand whether the reduction of inflammation was determined through the disruption of the LPS/CD44/NF-kB pathway, we evaluated the NF-kB translocation into the nucleus in the experimental groups. Finally, we implanted subcutaneously in rats' CSCL and CL scaffolds to understand whether the presence of CS onto the scaffold could help tuning the inflammation also in an in vivo setting. We selected the 72-h time points the most indicative of macrophages retention[21] as well as of the completion of the inflammatory phase.

Materials and methods

Scaffold preparation

CL scaffolds were fabricated with the freeze-dry technique previously reported.[22] Briefly, we prepared an acetic collagen type I (Nitta) slurry (10 mg/mL), which was precipitated to pH 5.5 with NaOH (1.67 mM). The material underwent wet crosslinking in an aqueous solution of 1,4-butanediol diglycidyl ether (BDDGE) (2.5 mM), at 4°C for 24 h. Finally, the slurry was washed with milli Q water scaffolds and prepared through a freeze-drying process. Chondroitin sulfate (Carbosynth) was added at the collagen solution at a weight molar ratio of 10:1 (CL:CS). After thorough mixing, the material was crosslinked and the final slurry was poured onto a 24-well plate and freeze dried. Scaffolds were air dried and sterilized by ultraviolet (UV) irradiation for 30 min inside a laminar flow hood and equilibrated in culture medium at 37°C for 5 h before use.

Scaffold characterization

Scanning electron microscope. Scaffolds were dehydrated by treatment with graded ethanol solutions (30%, 50%, 75%, 85%, and 95% each for 2 h) and then placed overnight in a dryer at room temperature (RT) before being coated with 7 nm of Pt/Pl for scanning electron microscope (SEM; FEI Nova NanoSEM 230) examination. The pore diameter of scaffolds was measured from SEM images, and five images were used for each scaffold. For each image, 20 different pores were randomly selected and their diameters measured using ImageJ software.

CL and CSCL were placed in OCT, frozen in liquid nitrogen, and cryosectioned at 7 μm. Ten sections for each material were placed on glass slides and allowed to dry at RT. Wheat germ agglutinin–fluorescein isothiocyanate (WGA-FITC) (Sigma–Aldrich) were applied to the sections at concentrations of 10 μg/mL in phosphate-buffered saline (PBS) containing 0.1% bovine serum albumin (BSA) for 1 h at RT.[23] All slides were washed four times with the PBS solution, gently blotted, mounted in cytosolix, and viewed by Nikon Histological Microscope using the appropriate filter sets. The quantification was carried on by Nikon Element Software.

BMDM isolation

BMDM were isolated as previously reported[24] for mouse and slightly adjusted for rat. After sacrificing Lewis rats, femurs were cleaned of surrounding tissues and cut at both ends. The cavity was flushed with complete media, using a 5-mL syringe and a 25-gauge needle. Bone marrow cells were mechanically separated into single-cell suspensions, filtered, and plated in media supplemented with macrophage colony-stimulating factor (10 ng/mL).

Once obtained, 3×10^5 rat macrophages were seeded onto CL and CSCL scaffolds—with a diameter of 0.8 cm and thickness 0.2 mm—in a concentrated drop of 50 μL on top of the dry scaffolds and allowed to adhere for 20 min, before media (up to 2 mL) was added. Cultures were established in high glucose–Dulbecco's Modified Eagle Medium (HG-DMEM) supplemented with 10% fetal bovine serum (FBS, v/v), and 1% penicillin (100 UI/mL)-streptomycin (100 mg/mL) and 0.25 mg/mL amphotericin B (v/v) at 37°C in a humidified atmosphere (90%) with 5% CO_2.

Cell morphology and distribution

After 24 h, cells grown onto CL and CSCL scaffolds were imaged by confocal microscopy or fixed and visualized by SEM. Samples (n=3 per group) were prepared by fixing cells in 4% paraformaldehyde, stained with a fluorescent Live-Dead Viability Assay (Molecular Probes, Eugene), and imaged by confocal microscopy (NIS-Elements software, Nikon), visualized in red for a better contrast with the blue background of the scaffold. Scanning electron microscopy (SEM) samples (n=3 per group) were first washed twice with 0.1 M sodium cacodylate buffer for

10 min. All samples were fixed with glutaraldehyde 2.5% w/v and paraformaldehyde 1% w/v in PBS (pH 7.4) (Electron Microscopy Sciences) overnight at 4°C. Dehydration was achieved using a graded series of ethanol (25%, 50%, 70%, 90%, and 100% for 10 min each). Specimens were mounted on metal stubs and stored in a vacuum desiccator for 48 h. In order to perform SEM analysis (FEI Quanta 400 ESEM FEG), samples were sputter-coated with 7 nm of Pt/Pd with Plasma Sciences CrC-150 Sputtering System (Torr International, Inc) and imaged with 10 kV. Quantification of cell elongation was calculated by the analysis of SEM images performed with ImageJ software, and it has been defined as the length of the longest axis divided by the length of the short axis.

Inducing macrophages inflammation in an in vitro system

To define the optimal condition to induce inflammation in rat BMDM through the activation of the CD44 pathway, cells were cultured for 48 and 72 h[25] in the presence of LPS, at the nominal concentrations of 10, 50, and 100 ng/mL. Macrophages inflamed and not inflamed with LPS were grown in two-dimensional (2D) standard conditions and used as positive and negative controls, respectively. At the end of the exposure, cells were analyzed at a molecular level for their expression of *CD44* and pro-inflammatory markers, as reported below.

Effect of CSCL in primary macrophages in vitro

BMDM were cultured for 24 h to assess their immediate response to the material, indicating the foreign-body reaction, or treated with bacterial LPS (100 ng/mL; Sigma) for 72 h[26] to evaluate the anti-inflammatory potential of CSCL compared to CL. Untreated macrophages grown onto scaffolds for the same length of time were used as a control. Macrophages inflamed, or not, with LPS and grown in 2D standard conditions were used as positive and negative controls, respectively. The 100-ng/mL LPS was chosen over three concentrations, nominally, 10, 50, and 100 ng/mL, tested for their efficacy in inducing inflammation on rat BMDM (5000 cells/cm^2) grown in a monolayer. At 72 h, media from each experimental group (n = 3) was recovered and kept at −20°C for further analyses. Cells were lysed and anti- and pro-inflammatory gene expression analysis was performed in triplicate from independent cultures (n = 3). In parallel, independent experimental groups were set to determine NF-kB activity on LPS-treated cells grown onto CSCL or CL.

Gene expression analysis

At each time point, macrophages grown onto scaffolds were lysed using Trizol reagent (Invitrogen). DNAse (Sigma) treatment followed the reaction. RNA concentration and purity were measured using a NanoDrop ND1000 spectrophotometer (NanoDrop Technologies). The complementary DNA (cDNA) was synthesized from 1 μg total RNA, using the iScript retrotranscription kit (Bio-Rad Laboratories). Transcribed products were analyzed using commercially available mastermix, following appropriate target probes on an ABI 7500 Fast Sequence Detection System (Applied Biosystems, Foster City, CA) to evaluate the expression of

- Hyaluronan receptor (*CD44:* Rn00681157_m1) and toll-like receptor-4 (*TLR-4:* Rn00569848_m1);
- Pro-inflammatory genes: tumor necrosis factor-alpha (*TNF-α:* Rn01525859_g1), inducible nitric oxide synthase (*iNOS:* Rn00561646), interleukin 12-alpha (*IL-12α:* Rn00575112_m1), interleukin 1-beta (*IL-1β:* Rn00580432_m1), metalloprotease type-1 (*MMP-1:* Rn01486634_m1), and interleukin 6 (*IL-6:* Rn01410330_m1).
- Anti-inflammatory genes: arginase (*Arg:* Rn01469630_m1), mannose receptor 1 (*MRC1:* Rn01487342_m1), interleukin 10 (*IL-10:* Rn01483988_g1), and transforming growth factor-beta (*TGF-β:* Rn01536049_g1).

All quantitative polymerase chain reaction (qPCR) assays used were TaqMan Gene Expression Assays (Life Technologies, Grand Island, NY, USA). Gene expression was normalized to the level of glyceraldehyde 3-phosphate dehydrogenase (*Gapdh:* Rn01775763_g1). For anti- and pro-inflammatory genes, values were normalized to those obtained from their respective control groups (unstimulated cells). Gene expression performed on ex vivo samples was evaluated compared to subcutaneous tissues with no inflammation (baseline).

NF-kB activity assay

Nuclear fractions were isolated and subsequently analyzed for NF-kB activity as per the manufacturer's instructions using the NF-kB p50/p65 Transcription Factor Assay Kit (ABCAM, ab133128). Experimental groups included BMDM grown onto collagen-based scaffolds in presence and absence of CS in standard conditions or in case of inflammation (LPS 100 ng/mL).

Nitric oxide measurement

The presence of nitric oxide (NO; μM) in the culture supernatants was measured using a Nitric Oxide (total) detection kit (Enzo Life Sciences) following the manufacturer's instructions. The levels of NO released from LPS-inflamed BMDM seeded onto CL and CSCL were compared to those produced by not inflamed cells grown

onto CL or CSCL, respectively. The levels of nitric oxide released by inflamed and not inflamed BMDM cultured in 2D were measured for comparison.

In vivo studies

Adult Lewis rats (n = 3; Charles River Laboratories, Houston, TX, USA) were used for in vivo validation studies. All animals were maintained and used in conformity with the guidelines established by the American Association for Laboratory Animal Science and all procedures approved by the Houston Methodist Institutional Animal Care and Use Committee (IACUC). Rats received appropriate preoperative analgesia with weight-based subcutaneously injected buprenorphine and carprofen. Induction and maintenance anesthesia was provided using inhaled isoflurane gas and the dorsum of each animal was shaved from shoulder to hock. Under sterile conditions, three skin incisions were made on both sides of the dorsal midline of each animal and the pre-muscular, avascular subcutaneous plane was developed using blunt dissection. Into each subcutaneous pocket, we placed a 1-cm-diameter, 0.3-cm-thick scaffold (left side: CL, right side: CSCL) and all incisions were closed with wound clips. Post-operatively, rats were housed in individual cages, given food and water ad libitum and kept on a 12-h light–dark schedule in a typical fashion. Seventy-two h after implantation, animals were humanely euthanized and scaffold specimens were harvested and kept for further analyses.

Histological and immunohistochemical analysis

Following euthanasia, the implant sites with surrounding tissue were removed and immersed in 10% buffered formalin phosphate solution for 48 h. 10-μm-thick sections were deparaffinized twice in fresh xylene for 8–10 min and rehydrated sequentially with decreasing ethanol concentrations (100%, 95%, 90%, 80%, 70%) and distilled water (8–10 min for each step) and then stained by Masson's Trichrome Staining (Abcam) and finally analyzed by Nikon Histological Microscope. For the immunohistochemical analysis, slides were pretreated using a standard cycle of pressure cooker to unmask epitopes in antigen retrieval solution (0.1 M sodium citrate, pH 7.2). The slides were blocked for 1 hr at RT with 10% normal goat serum (NGS) and 0.03% Triton and then incubated at 4°C overnight with anti-macrophage antibody (ab7429 abcam). Slides were then washed three times in PBS and finally mounted with ProLong® Gold Antifade Reagent (with 4′,6-diamidino-2-phenylindole (DAPI)) (Invitrogen). Slides were stored at 4°C in the dark until imaging was performed by a Nikon Histological Microscope and the fluorescence quantification by Nikon Element software.

Statistical analysis

Statistical analysis was performed using GraphPad Instat 3.00 for Windows (GraphPad Software, La Jolla, CA, USA). Three replicates for each experiment were performed and the results are reported as mean ± standard deviation. $p \leq 0.05$ was considered as significant. A one-way analysis of variance (ANOVA) for multiple comparisons by Student–Newman–Keuls multiple comparison test was used.

Results

Material characterization

Ultrastructural analysis of the fabricated scaffolds was investigated by SEM. Figure 2(a) and (b) represents the CSCL structure that showed numerous interconnected pores, with smooth separation walls and irregular, but ovoid, shape and dimensions of approximately 80 μm × 60 μm. At higher magnification (Figure 2 (c) and (d)), these structures were resolved as randomly oriented, nano-sized collagen fibers that maintained the organized collagen ultrastructure. In order to assess whether the exposed CS could also exploit their biological signaling function upon recognition of their complementary receptor, conjugation with WGA on the CSCL was performed (Figure 2(e) and (f)). CSCL presence was evaluated by fluorescence microscopy and showed that the CS is on 18% ± 0.78% of the exposed scaffold's surface.

Effect of CSCL in primary macrophages in vitro

Confocal Microscopy of BMDM (Figure 3(a), red dots) showed that the distribution of living BMDM inside the scaffold appeared to be equally distributed along the scaffold walls (visualized in red for a better contrast with the blue background of the scaffold). The scaffold porosity allows the homogenous distribution of the cell across the scaffold thickness. Quantification of cell elongation was used to understand changes in macrophages' phenotype and has been defined as the length of the longest axis divided by the length of the short axis. Results showed a significantly higher presence (>~25%) of elongated cells on CSCL after 24 h in comparison with CL. Figure 3(a) displays how BMDM organize across CL and CSCL, while Figure 3(b) demonstrates the effect of CS on cell morphology. When cells were analyzed for the expression of anti- and pro-inflammatory markers, an increase in the expression of *TGF-β*, *Arg*, *MRC1*, and *IL-10* was noted in the CSCL experimental group with a concomitant decrease in the expression of *TNF-a* and *iNOS*. The expression of *IL-6* was found to be significantly (p < 0.01) higher in CSCL than CL. Figure 3(c) shows a heatmap comparing the expression of these markers on CL, CSCL, and cells cultured in 2D conditions. In this latter case, BMDM
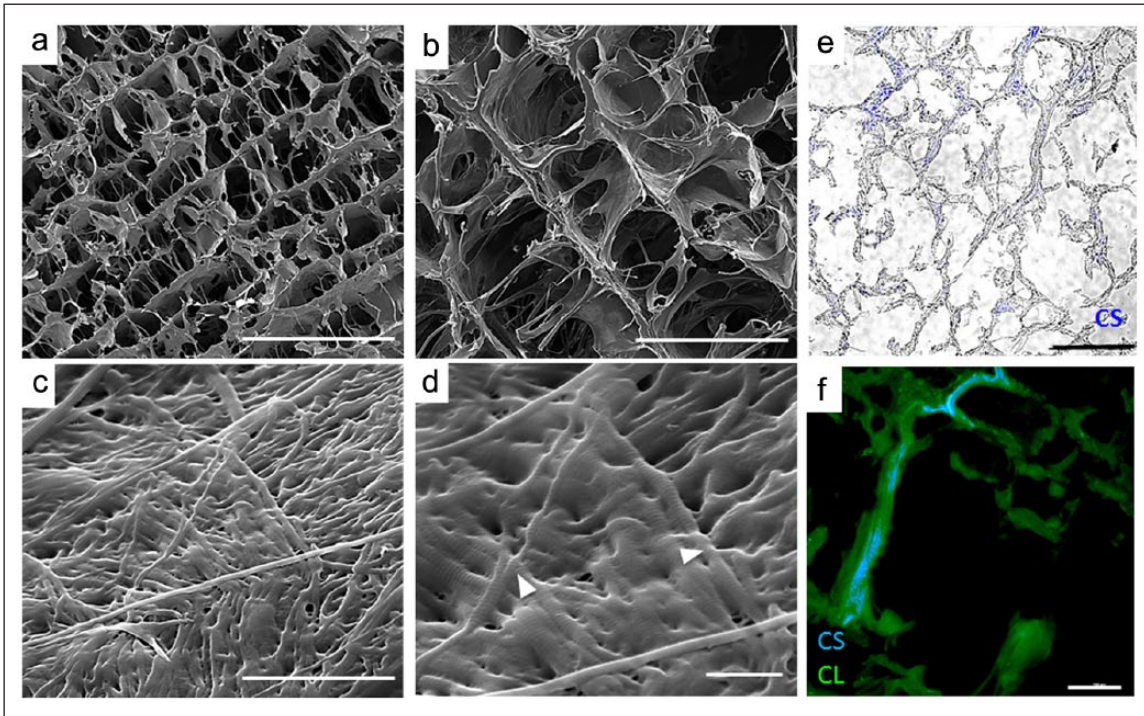
Figure 2. Scaffold characterization. (a, b) SEM micrographs showed highly porous structures with interconnected pores. (c, d) At higher magnification, the SEM reveals that collagenous scaffolds maintain the collagen ultrastructure (white arrows). (e, f) Scaffold slices were stained with WGA (wheat germ agglutinin). The 18% of fluorescence area indicates the exposure of chondroitin sulfate onto scaffold surface (blue signal).

treated with pro-inflammatory (TNF-α and IFN-γ) and anti-inflammatory cytokines (IL-10 and IL-4) are reported as positive controls.

In vitro optimization of the inflammatory system

To define the most striking conditions to induce inflammation in BMDM and assess the capability of CS immobilized into a collagen-based scaffold, cells were treated with different concentrations of LPS, nominally, 10, 50, and 100 ng/mL. Data are shown in Figure 4. At 72 h, the three concentrations were equally effective in inducing a significant increase in *CD44* expression compared to the control represented by BMDM grown in absence of LPS. The most efficient working concentration was the 10 ng/mL, showing an almost 29.28 (±2.04)-fold increase compared to the control. Data obtained following exposure to LPS, at the highest concentrations, were assessed around 24.86 (±4.5) and 24.29 (±0.41)-fold for the 50 and 100 ng/mL, respectively. When looking at the pro-inflammatory marker expression, although a significant increase was demonstrated following all treatments, the 100-ng/mL concentration resulted in the most prominent induction, with a 67.221 (±39.94)-, 4,307 (±6.56)-, 54.67 (±6.38)-, 31.98 (±6.5)-, and 486.86 (± 18.79)-fold increase for *TNF-α, iNOS, IL-1β, IL-12β*, and

MMP-1, respectively. No significant induction was found at 48 h (data not shown).

Role of CS in reducing inflammation

To study our CSCL scaffold's ability to reduce inflammation, BMDM were grown onto CL and CSCL and stimulated for 72 h with 100 ng/mL LPS. Figure 5(a) shows a schematic representation of the experimental design. A significant reduction in the expression of *CD44*, *TNF-α*, *iNOS*, *IL-1β*, *IL-12β*, and *MMP-1* was found when BMDM were grown onto CSCL and exposed to LPS, compared to cells cultured in 2D conditions or onto CL. Interestingly, *CD44* expression was found to increase 9.90 (±0.31)-fold in CL but only 4.43 (±0.05)- fold in CSCL. Following exposure to LPS, the presence of CS on the scaffold is linked to a striking reduction in the expression of pro-inflammatory genes (*iNOS, TNF-α, IL-1β, IL-12β*, and *MMP-1*), showing values that, in most cases, were comparable to those observed in the controls (Figure 5(b)). We further evaluated nitrate concentrations in the culture supernatant and found a significant difference between CSCL and CL in both conditions, especially after LPS exposure (Figure 5(c)) in which the nitrate concentration is almost 10 times less in comparison with CL.
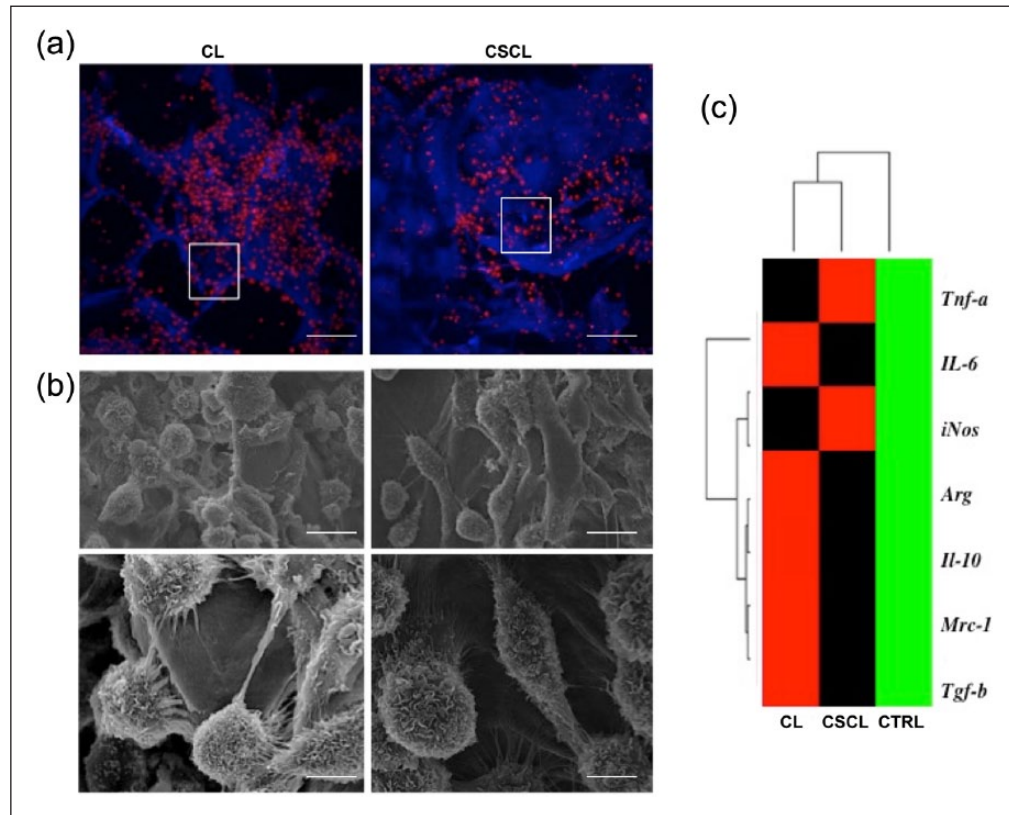
Figure 3. Reaction to the scaffold. (a) Confocal images showing macrophages spread onto CL and CSCL scaffolds. (b) SEM images showing how the presence of CS affects cell morphology. (c) Heatmap of differentially expressed genes between CSCL and CL in vitro. Pro- (*TNF-α*, *IL-6*, and *iNOS*) and anti- (*Arg*, *IL-10*, *MRC1*, and *TGF-β*) inflammatory markers are shown. Expression levels of genes are displayed as color codes. Red represents over-expression while green under-expression. Black represents expression levels not significantly different to the control (CTRL), represented by BMDM grown in 2D conditions. Genes were clustered according to their distance determined by Pearson's correlation.

To validate these data, NF-kB nuclear translocation analysis was performed in parallel with the same experimental groups. NF-kB activity was demonstrated in 100 ng/mL LPS-treated BMDM (positive control), as well as in inflamed cells grown onto CL scaffolds. Data obtained from cells cultured onto CSCL and inflamed with LPS were comparable to the controls (untreated cells) (Figure 5(d)).

In vivo data

In vivo cellular infiltration was observed on both scaffolds (Figure 6). Macrophages were able to infiltrate through the whole scaffolds' thickness and were found in the explants at 72 h (Figure 6(a) and (b)). However, at the surgical implant interface (dotted yellow line), CL showed a strong mononuclear cell response at 72 h in comparison with CSCL (Figure 6(a)–(d)). In both cases, no multinucleated giant cells were detected and there was no evidence of alteration to surrounding tissues. The immunohistochemical analysis (Figure 6(e) and (f)) highlighted a higher infiltration of macrophages along all the CSCL scaffold thickness in comparison with CL (Figure 6(g)). At a molecular level, qPCR analysis shows a downregulation in the expression of the surface receptor *CD44*, with the consequent reduction of the pro-inflammatory markers studied (*TNF-α*, *iNOS*, *IL-12β*, *IL-1β*, and *MMP-1*) (Figure 6(h)).

Discussion

The inflammatory response to a biomaterial is one of the key factors determining the remodeling outcome.[27] Typically, the inflammatory response to an implanted biomaterial is characterized by a well-described sequence of events that could either result in tissue restoration or foreign-body giant-cell formation and fibrosis at the host–implant interface.[28] The most important cellular players in these events are the mononuclear phagocyte cells that have been described in two different states of polarization, proinflammatory, and anti-inflammatory macrophages (called M1 and M2, respectively).[29,30] The pro-inflammatory, M1, are associated with the classic signs of inflammation in the cytokines/chemokines expression pattern, whereas the
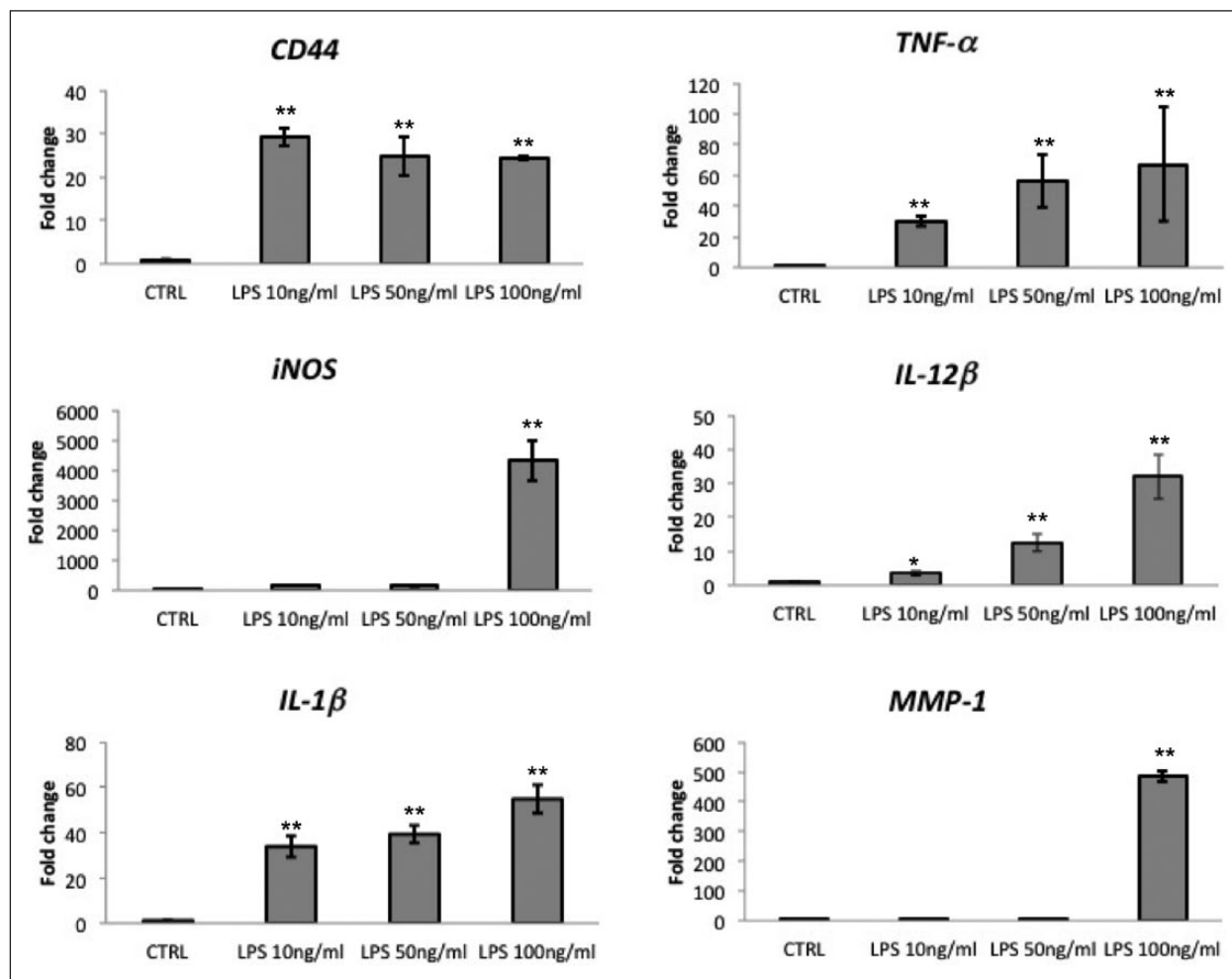
Figure 4. Expression of pro-inflammatory markers activated by LPS. Graphs represent the expression of the surface marker *CD44* and the pro-inflammatory markers (*TNF-α, iNOS, IL-12β, IL-1β*, and *MMP-1*) in BMDM following exposure to nominal concentrations of LPS (10, 50, and 100 ng/mL) for 72 h. Expression levels have been determined by quantitative RT-PCR. Data were normalized to the reference gene (*Gapdh*) and represented as fold-change compared with the expression observed untreated BMDM (CTRL). Values are mean ± SD (n = 3). Asterisks depict highly significant (**p < 0.01) differences.

anti-inflammatory, M2, phenotype promotes immunomodulation toward tissue remodeling. Besides such dualism, it has been reported that macrophages are highly plastic cells, able to switch from the M1 to the M2 phenotype, and vice-versa when appropriately stimulated.[31] Very few biomaterials focus on the M1 to M2 polarization in vitro, and even fewer in vivo,[32] due to the complexity of the system. Surface topography, molecular organization, and composition of biomaterials have shown to clearly affect macrophage polarization, directing downstream remodeling events.[33–36] However, understanding macrophage reaction at the implant site still remains complicated. In fact, it is a combination of two distinct events that occur at the same time: the inflammation phase caused by the injury and the reaction caused by the presence of the implant.

The current study is aimed at recapitulating the two separate events in vitro to better understand the mechanisms activated by the implant of a biomaterial because

distinguishing the two reactions is not feasible in an in vivo setting. We studied the reaction of BMDM to a scaffold functionalized with an immunotuning macromolecule, the CS, to control the inflammatory reaction through the surface chemistry of the biomaterial.

To understand the bare scaffold reaction, BMDM have been seeded onto CSCL. Data obtained from this study suggest that the presence of CS is responsible for BMDM elongation, which correlates to an increased expression of M2-specific markers in CSCL compared to CL.[37,38] In fact, elongated macrophages expressed higher levels of *Arg-1, IL-10, MRC1*, and *TGF-β*. At the same time, pro-inflammatory marker expression was significantly reduced. *IL-6* was the only gene found overexpressed, although its induction can be explained by the presence of the isoform A of the chondroitin crosslinked to the collagen.[39] To further prove the effectiveness of the system in supporting a regeneration-permissive environment by preventing LPS-CD44
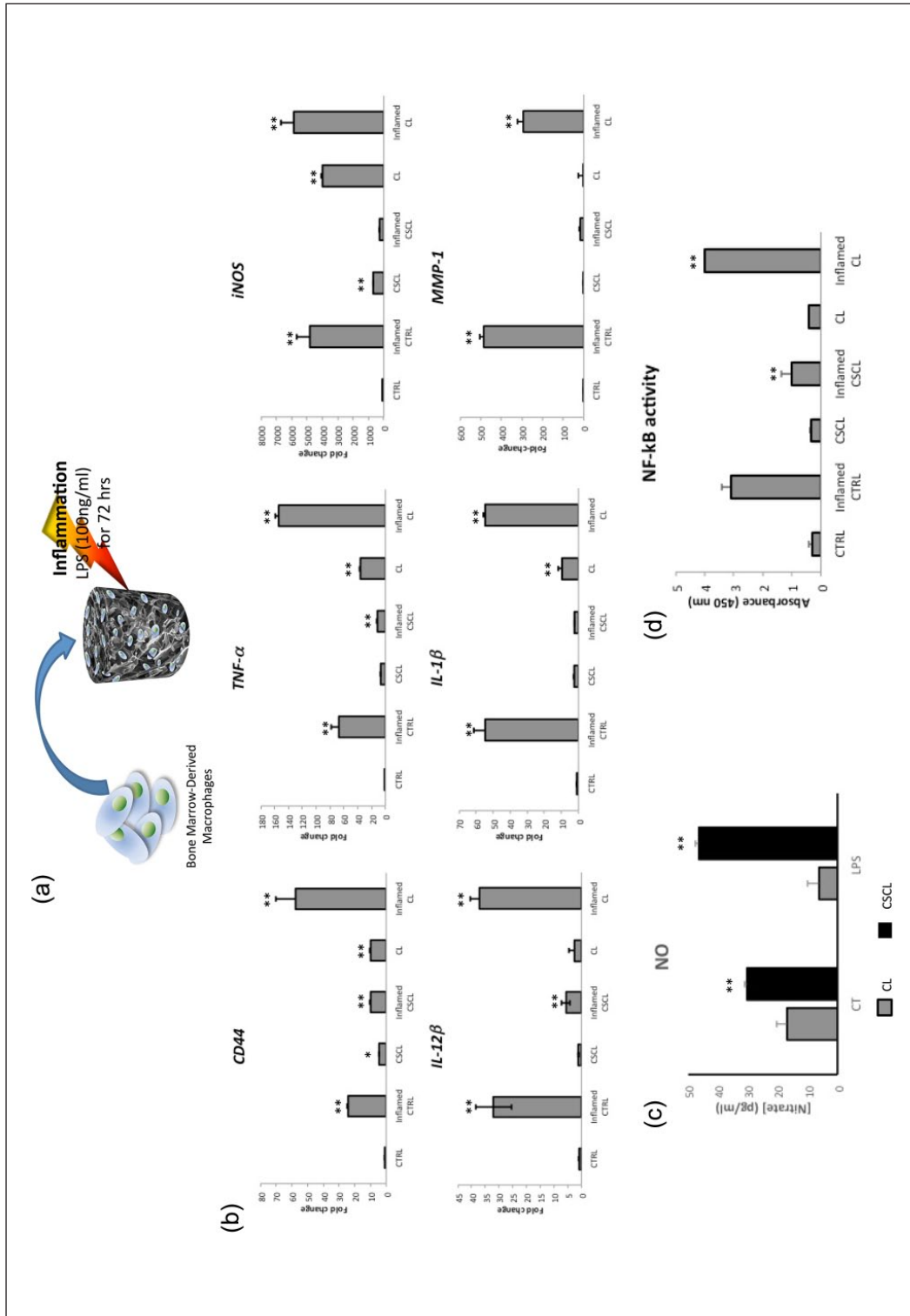
Figure 5. CS potential to reduce inflammation. (a) Schematic representation of the experimental design. BMDM were seeded onto CSCL or CL scaffolds and inflamed for 72 h with LPS (100 ng/ml). (b) Graphs representing the expression of the surface marker *CD44* and pro-inflammatory markers (*TNF-α, iNOS, IL-12β, IL-1β,* and *MMP-1*) at 72 h. Expression levels have been determined by quantitative RT-PCR. Data were normalized to the reference gene (*Gapdh*) and represented as fold-change compared with the expression observed untreated BMDM (CTRL). The expression of pro-inflammatory genes in cells treated with LPS (100 ng/mL; inflamed) and cultured in 2D conditions is reported for comparison. Values are mean ± SD (n = 3). Asterisks depict highly significant (**p < 0.01) and significant (*p < 0.05) differences compared to control. (c) Nitrate concentration in the cell culture media of BMDM grown onto CSCL and CL at 72 h. Asterisks depict highly significant (*p < 0.01) differences. (d) NF-kB activity as a measure of nuclear translocation. Assay of cell lysates isolated from inflamed and not inflamed cells grown in 2D conditions (inflamed CTRL and CTRL, respectively) and from cells grown onto CSCL and CL in presence (inflamed) or absence of LPS, demonstrating NF-kB p65 activity. Values are mean ± SD (n = 3). Asterisks depict highly significant (**p < 0.01) differences compared to inflamed CTRL.
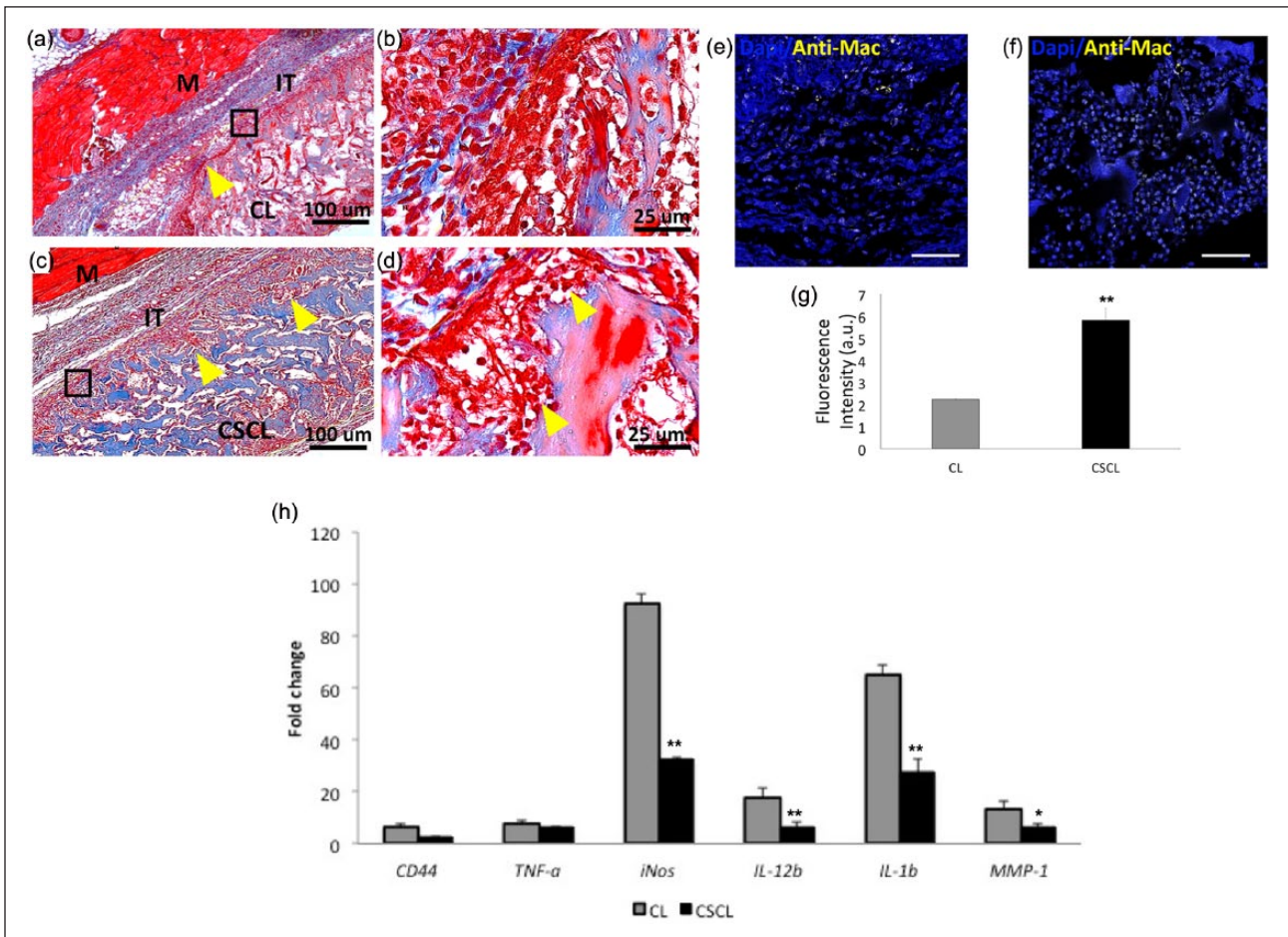
Figure 6. In vivo analysis of scaffolds implanted in rat's subcutaneous pouch after 72 h. Masson's trichrome staining of ((a) CL, (c) CSCL) the entire scaffold and ((b) CL, (d) CSCL) and their magnification. The CL scaffold shows an ongoing infiltration of leukocytes along the entire scaffold thickness in comparison with CSCL. In the histological section, we indicated the muscular subcoutaneous fascia (M) and the interface tissue surrounding the implanted scaffold (IT). Low magnification images: scale bars = 300 μm; insets = 20 μm. Immunofluorescence staining of macrophages (yellow) infiltrating the (e) CL and (f) CSCL scaffolds in a subcutaneous implant model. (g) Data are quantified as mean fluorescence intensity and showed as comparison between CSCL and CL. Scale bar = 50 μm. (h) Graph representing the expression of the surface marker *CD44* and Pro- (*TNF-α*, *iNOS*, *IL-12β*, *IL-1β*, and *MMP-1*) at 72 h from in vivo implant. Expression levels have been determined by quantitative RT-PCR. Data were normalized to the reference gene (*Gapdh*) and represented as fold-change compared with the expression observed in a not inflamed tissue (baseline). Asterisks depict highly significant (**$p < 0.01$) and significant (*$p < 0.05$) differences compared to CL.

binding, we identified in the 100-ng/mL the optimal LPS concentration to induce a significant upregulation in pro-inflammatory genes (*TNF-α*, *iNOS*, *IL-12β*, *IL-1β*, and *MMP-1*). BMDM were then seeded onto scaffolds and exposed to LPS for 72 h. Our in vitro data confirmed that CS interferes with the activation of the LPS/CD44/NF-kB cascade leading to the reduction of the downstream pro-inflammatory genes.[20] Along with pro-inflammatory genes, following inflammation macrophages usually release NO as a way to kill pathogens.[40,41] Furthermore, NO is known to mediate the inflammatory response by inhibiting or inducing inflammation via a variety of different pathways.[42–44] We proved that CS prevents NO release under normal and inflamed conditions in comparison with CL,

showing its immunomodulatory potential. Inflamed macrophages grown onto CSCL scaffold showed a downregulation in the expression of CD44, with a concomitant reduction in the Nf-kb activity, which ultimately led to reduced levels of pro-inflammatory messenger RNA (mRNA) compared to the positive control (LPS-induced cells in 2D conditions) and to the inflamed CL. In vivo studies supported our in vitro findings, showing an overall decrease in the levels of mRNA associated with pro-inflammatory genes in CSCL scaffolds after 72 h from implant. Histological sections further supported these observations, showing higher infiltration of macrophages after 72 h, suggesting an earlier termination of the inflammatory process around the CSCL implant.[45,46]

Although statistically significant differences have been observed between CL and CSCL, it is worth noting that a residual inflammation is still present also in presence of CS. According to the literature, LPS-inflammatory activity relies also on the induction of an alternative molecular pathway able to upregulate pro-inflammatory gene expression. Such activation is also mediated by the capability of LPS to bind another receptor on macrophages surface, the TLR-4.[47,48] In the process of understanding the data obtained from our in vitro testing, we analyzed the expression of the gene *TLR-4* following macrophages exposure to different concentrations of LPS, showing a 11.06 ($\pm$2.5)-fold increase at 100 ng/mL (Supplementary Information 1).
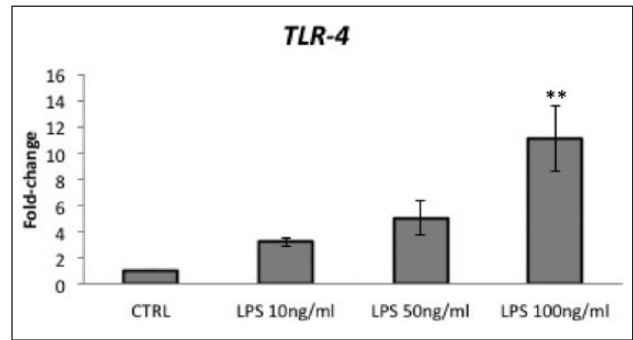
Taken together, our results suggest the role of our CSCL scaffold in moderating the inflammatory response to an implant, both in vitro and in vivo. Its ability to interfere with the activation of the CD44/NF-kB signaling[49,50] makes it suitable for clinical applications in the treatment of diseases caused by cartilage degeneration, including osteoarthritis.[20] Literature reports previous observations regarding the role CD44 plays in preventing exaggerated inflammatory responses to LPS by promoting the negative regulation of the TLR-4 signaling in macrophages in the context of pulmonary inflammation.[51] Additional analyses focusing to elucidate the mechanisms by which CS could improve the CD44-mediated modulation of inflammation could lead to the development of new therapeutic approaches.

Conclusion

The understanding of macrophage polarization and its role in wound healing is increasing its importance in developing innovative, cutting-edge tissue-engineering approaches. We have shown that a cell-free, CS-functionalized collagen scaffold is able to tune macrophage polarization by exploiting the same molecular pathway (LPS/CD44/NF-kB), both in vitro and in vivo. The recent advances in the description of the role of inflammatory cells will provide new insights when designing novel immunoinformed biomaterials aimed at functional tissue restoration.

Supplementary Information 1

Expression of TLR-4 following treatment with different concentrations of LPS. Graph represents the expression of the surface marker *TRL-4* in BMDM following exposure to nominal concentrations of LPS (10, 50, and 100 ng/mL) for 72 h. Expression levels have been determined by quantitative RT-PCR. Data were normalized to the reference gene (*Gapdh*) and represented as fold-change compared with the expression observed untreated BMDM (CTRL). Values are mean $\pm$ SD (n = 3). Asterisks depict highly significant (**p < 0.01) differences.

Author's Note

Francesca Taraballi and Bruna Corradetti equally contributed to this article.

References

1. Eshghi S and Schaffer DV. Engineering microenvironments to control stem cell fate and function, 2008, http://www.ncbi.nlm.nih.gov/books/NBK27048/
2. Baiguera S, Urbani L and Del Gaudio C. Tissue engineered scaffolds for an effective healing and regeneration: reviewing orthotopic studies. *Biomed Res Int* 2014; 2014: 398069.
3. Willerth SM and Sakiyama-Elbert SE. Combining stem cells and biomaterial scaffolds for constructing tissues and cell delivery, 2008, http://www.ncbi.nlm.nih.gov/books/NBK27050/
4. Chen F-M, Wu L-A, Zhang M, et al. Homing of endogenous stem/progenitor cells for in situ tissue regeneration: promises, strategies, and translational perspectives. *Biomaterials* 2011; 32(12): 3189–3209.
5. Lane SW, Williams DA and Watt FM. Modulating the stem cell niche for tissue regeneration. *Nat Biotechnol* 2014; 32: 795–803.
6. Higuchi A, Ling Q-D, Chang Y, et al. Physical cues of biomaterials guide stem cell differentiation fate. *Chem Rev* 2013; 113(5): 3297–3328.

7. Chew SY and Low WC. Scaffold-based approach to direct stem cell neural and cardiovascular differentiation: an analysis of physical and biochemical effects. *J Biomed Mater Res A* 2011; 97(3): 355–374.

8. Lee K, Silva EA and Mooney DJ. Growth factor delivery-based tissue engineering: general approaches and a review of recent developments. *J R Soc Interface* 2011; 8(55): 153–170.

9. Jiang J and Papoutsakis ET. Stem-cell niche based comparative analysis of chemical and nano-mechanical material properties impacting ex vivo expansion and differentiation of hematopoietic and mesenchymal stem cells. *Adv Healthc Mater* 2013; 2(1): 25–42.

10. Kao WJ. Evaluation of protein-modulated macrophage behavior on biomaterials: designing biomimetic materials for cellular engineering. *Biomaterials* 1999; 20(23): 2213–2221.

11. Brown BN, Ratner BD, Goodman SB, et al. Macrophage polarization: an opportunity for improved outcomes in biomaterials and regenerative medicine. *Biomaterials* 2012; 33(15): 3792–3802.

12. Murray PJ, Allen JE, Biswas SK, et al. Macrophage activation and polarization: nomenclature and experimental guidelines. *Immunity* 2014; 41(1): 14–20.

13. Vasconcelos DP, Costa M, Amaral IF, et al. Modulation of the inflammatory response to chitosan through M2 macrophage polarization using pro-resolution mediators. *Biomaterials* 2015; 37: 116–123.

14. Vasconcelos DP, Costa M, Amaral IF, et al. Development of an immunomodulatory biomaterial: using resolvin D1 to modulate inflammation. *Biomaterials* 2015; 53: 566–573.

15. Watanabe H, Yamada Y and Kimata K. Roles of aggrecan, a large chondroitin sulfate proteoglycan, in cartilage structure and function. *J Biochem* 1998; 124(4): 687–693.

16. Ronca F, Palmieri L, Panicucci P, et al. Anti-inflammatory activity of chondroitin sulfate. *Osteoarthritis Cartilage* 1998; 6: 14–21.

17. Clegg DO, Reda DJ, Harris CL, et al. Glucosamine, chondroitin sulfate, and the two in combination for painful knee osteoarthritis. *N Engl J Med* 2006; 354(8): 795–808.

18. Iovu M, Dumais G and Du Souich P. Anti-inflammatory activity of chondroitin sulfate. *Osteoarthritis Cartilage* 2008; 16: S14–S18.

19. Monfort J, Pelletier J-P, Garcia-Giralt N, et al. Biochemical basis of the effect of chondroitin sulphate on osteoarthritis articular tissues. *Ann Rheum Dis* 2008; 67(6): 735–740.

20. Loeser RF, Yammani RR, Carlson CS, et al. Articular chondrocytes express the receptor for advanced glycation end products: potential role in osteoarthritis. *Arthritis Rheum* 2005; 52(8): 2376–2385.

21. Sridharan R, Cameron AR, Kelly DJ, et al. Biomaterial based modulation of macrophage polarization: a review and suggested design principles. *Mater Today* 2015; 18: 313–325.

22. Minardi S, Sandri M, Martinez JO, et al. Multiscale patterning of a biomimetic scaffold integrated with composite microspheres. *Small* 2014; 10(19): 3943–3953.

23. Taraballi F, Russo L, Battocchio C, et al. A model study for tethering of (bio) active molecules to biomaterial surfaces through arginine. *Org Biomol Chem* 2014; 12(24): 4089–4092.

24. Weischenfeldt J and Porse B. Bone marrow-derived macrophages (BMM): isolation and applications. *CSH Protocol* 2008; 2008(12): pdb.prot5080.

25. Yan B, Xie S, Liu Z, et al. HDAC6 deacetylase activity is critical for lipopolysaccharide-induced activation of macrophages. *PLoS ONE* 2014; 9: e110718.

26. Ruffell B, Poon GF, Lee SS, et al. Differential use of chondroitin sulfate to regulate hyaluronan binding by receptor CD44 in inflammatory and interleukin 4-activated macrophages. *J Biol Chem* 2011; 286(22): 19179–19190.

27. Badylak SF, Valentin JE, Ravindra AK, et al. Macrophage phenotype as a determinant of biologic scaffold remodeling. *Tissue Eng Part A* 2008; 14(11): 1835–1842.

28. Anderson JM, Rodriguez A and Chang DT. Foreign body reaction to biomaterials. *Semin immunol* 2008; 20: 86–100.

29. Gordon S and Taylor PR. Monocyte and macrophage heterogeneity. *Nat Rev Immunol* 2005; 5(12): 953–964.

30. Mantovani A, Sica A and Locati M. Macrophage polarization comes of age. *Immunity* 2005; 23(4): 344–346.

31. Geissmann F, Gordon S, Hume DA, et al. Unravelling mononuclear phagocyte heterogeneity. *Nat Rev Immunol* 2010; 10(6): 453–460.

32. Zhang L, Cao Z, Bai T, et al. Zwitterionic hydrogels implanted in mice resist the foreign-body reaction. *Nat Biotechnol* 2013; 31(6): 553–556.

33. Jones JA, Chang DT, Meyerson H, et al. Proteomic analysis and quantification of cytokines and chemokines from biomaterial surface-adherent macrophages and foreign body giant cells. *J Biomed Mater Res A* 2007; 83(3): 585–596.

34. Luttikhuizen D, Dankers P, Harmsen M, et al. Material dependent differences in inflammatory gene expression by giant cells during the foreign body reaction. *J Biomed Mater Res A* 2007; 83(3): 879–886.

35. Courtman DW, Errett BF and Wilson GJ. The role of crosslinking in modification of the immune response elicited against xenogenic vascular acellular matrices. *J Biomed Mater Res* 2001; 55(4): 576–586.

36. Liang H-C, Chang Y, Hsu C-K, et al. Effects of crosslinking degree of an acellular biological tissue on its tissue regeneration pattern. *Biomaterials* 2004; 25(17): 3541–3552.

37. Johnson JL and Newby AC. Macrophage heterogeneity in atherosclerotic plaques. *Curr Opin Lipidol* 2009; 20(5): 370–378.

38. Jay SM, Skokos E, Laiwalla F, et al. Foreign body giant cell formation is preceded by lamellipodia formation and can be attenuated by inhibition of Rac1 activation. *Am Journal Pathol* 2007; 171(2): 632–640.

39. Jin M, Iwamoto T, Yamada K, et al. Disaccharide derived from chondroitin sulfate A suppressed CpG-induced IL-6 secretion in macrophage-like J774. 1 cells. *Cytokine* 2010; 51(1): 53–59.

40. Maugé L, Fotopoulou T, Delemasure S, et al. In vitro inflammatory/anti-inflammatory effects of nitrate esters of purines. *Eur J Pharmacol* 2014; 730: 148–156.

41. Nathan CF and Hibbs JB. Role of nitric oxide synthesis in macrophage antimicrobial activity. *Curr Opin Immunol* 1991; 3(1): 65–70.

42. Rubbo H, Parthasarathy S, Barnes S, et al. Nitric oxide inhibition of lipoxygenase-dependent liposome and low-density lipoprotein oxidation: termination of radical chain propagation

reactions and formation of nitrogen-containing oxidized lipid derivatives. *Arch Biochem Biophys* 1995; 324(1): 15–25.

43. McInnes IB, Leung BP, Field M, et al. Production of nitric oxide in the synovial membrane of rheumatoid and osteoarthritis patients. *J Exp Med* 1996; 184(4): 1519–1524.

44. Kuo H-P, Wang C-H, Huang K-S, et al. Nitric oxide modulates interleukin-1 β and tumor necrosis factor-α synthesis by alveolar macrophages in pulmonary tuberculosis. *Am J Resp Crit Care* 2000; 161(1): 192–199.

45. Laschke M, Strohe A, Scheuer C, et al. In vivo biocompatibility and vascularization of biodegradable porous polyurethane scaffolds for tissue engineering. *Acta Biomater* 2009; 5(6): 1991–2001.

46. Blackwell NM, Sembi P, Newson JS, et al. Reduced infiltration and increased apoptosis of leukocytes at sites of inflammation by systemic administration of a membrane-permeable IκBα repressor. *Arthritis Rheum* 2004; 50(8): 2675–2684.

47. Akira S and Takeda K. Toll-like receptor signalling. *Nat Rev Immunol* 2004; 4(7): 499–511.

48. Liew FY, Xu D, Brint EK, et al. Negative regulation of toll-like receptor-mediated immune responses. *Nat Rev Immunol* 2005; 5(6): 446–458.

49. Fujimoto T, Kawashima H, Tanaka T, et al. CD44 binds a chondroitin sulfate proteoglycan, aggrecan. *Int Immunol* 2001; 13(3): 359–366.

50. Croft DR, Dull P, Davies D, et al. Complex CD44 splicing combinations in synovial fibroblasts from arthritic joints. *Eur J Immunol* 1997; 27(7): 1680–1684.

51. Liang J, Jiang D, Griffith J, et al. CD44 is a negative regulator of acute pulmonary inflammation and lipopolysaccharide-TLR signaling in mouse macrophages. *J Immunol* 2007; 178(4): 2469–2475.